In Situ Time-Resolved Phase Evolution and Phase Transformations in U-6 Wt Pct Nb

JIANZHONG ZHANG, DONALD W. BROWN, BJORN CLAUSEN, SVEN C. VOGEL, and ROBERT E. HACKENBERG

In situ time-resolved synchrotron X-ray diffraction experiments were conducted to study the fine-scale phase evolution of U-6Nb. Upon rapid heating from 125 °C to 400 °C, a reverse martensitic transformation sequence, $\alpha'' \rightarrow \gamma^{o} \rightarrow \gamma_s$, was observed in less than 4 seconds, which represents the first direct observation of the $\gamma^{o} \rightarrow \gamma_s$ transformation in diffraction-based measurements. Consistent with previous *ex situ* metallography experiments, our isothermal hold experiments at 526 °C, 530 °C and 565 °C reveal two distinct reactions for the phase separation, $\gamma_s \rightarrow \alpha\text{-U} + \gamma_1$ (general precipitation) followed by $(\alpha\text{-U} + \gamma_1) \rightarrow \alpha\text{-U} + \gamma_{1\text{-}2}$ (discontinuous precipitation). For the first-stage precipitation, the incubation time is determined to be ~ 50 and 100 seconds, respectively, for the isothermal aging at 526-530 °C and 565 °C. At this stage, the phase transformation is characterized by the simultaneous growth of α-U and γ_1 at the expense of γ_s. As expected from the Arrhenius equation for the reaction rate, the determined times (~ 23 minutes) for the completion of the first-stage reaction at 526 ± 3 °C and 530 ± 3 °C are nearly twice longer than that at 565 ± 4 °C (~ 13 minutes). Over these periods of time, the Nb contents derived from a Vegard's-type relationship for γ_1 are in the 30.2 to 32.1 and 29.2 to 30.6 at. pct ranges, and the kinetics of the precipitation at 565 ± 4 °C can be described by the classic Avrami rate equation and one-dimensional growth of a surface or grain-boundary nucleation. During the second-stage precipitation, the γ_1 phase continues to enrich in Nb as it gradually evolves toward the $\alpha + \gamma_{1\text{-}2}$ metastable state (up to 47 at. pct over a period of 172 minutes at 530 °C). These new and time-resolved measurements can be used to better constrain the time–temperature–transformation diagram, solute (Nb) redistribution, and transformation kinetics during the early stages of the diffusional phase transformation.

https://doi.org/10.1007/s11661-019-05212-1

I. INTRODUCTION

THE uranium-niobium system is a complex system with numerous competing stable and metastable phases as a function of temperature and composition at atmospheric pressure. Depending on the Nb concentration, the U-Nb alloys exhibit several non-equilibrium structures upon rapid quenching from the high-temperature, Nb-supersaturated bcc γ_s phase to ambient temperature: orthorhombic α' phase at 0 to 4.2 wt pct Nb, monoclinic α'' phase at 4.2 to 6.9 wt pct, and tetragonal γ^{o} phase at 6.9 to 8.9 wt pct, using the notation suggested by Lehmann and Hills.[1] The α' structure is similar to pure α-uranium but with altered lattice parameters, whereas the α'' and γ^{o} structures are distorted α-U and γ-U, respectively. At elevated temperatures above 300 °C all metastable phases of the U-Nb alloys would eventually evolve toward or decompose into the $\alpha + \gamma_2$ final equilibrium state, where γ_2 is a Nb-rich bcc phase, commonly accepted to contain ~ 75 at. pct Nb at equilibrium.[2,3] Of particular interest are the U-Nb alloys near 6 wt pct niobium, *aka* U-6Nb, because the properties that make U-Nb alloys attractive for nuclear applications, such as oxidation resistance and ductility,[4] are optimized in this solute composition. Owing to the diffusionless martensitic mechanism intrinsic to its formation, the monoclinic U-6Nb structure is thermodynamically metastable and is expected to decompose as it is aged or subject to external stimuli such as thermal activation and mechanical perturbation.[5,6] A common issue of concern in these applications is the impact of long-term aging, thermal

JIANZHONG ZHANG, DONALD W. BROWN, BJORN CLAUSEN, and SVEN C. VOGEL are with the Material Science and Technology Division, Los Alamos National Laboratory, Los Alamos, NM 87545. Contact e-mail: jzhang@lanl.gov ROBERT E. HACKENBERG is with the SIGMA Division, Los Alamos National Laboratory.

Manuscript submitted December 12, 2018.
Article published online April 5, 2019

Table I. Detailed Time Information for the General Precipitation During Cooling and Early Stages of Isothermal Aging

Aging T (°C)	t_1 (s)	Cooling Rate (°C/s)	GP Start Time/T	GP End Time (s)	t_2 (s)
530 ± 3	98	1.20	49 s/541 °C	1441	1392
526 ± 3	99	1.22	51 s/535 °C	1436	1386
565 ± 4	99	0.79	99 s/569 °C	874	775

t_1: the elapsed time between 647 °C and an aging temperature during cooling, t_2: the time difference between the start and end of general precipitation (GP), *i.e.*, $\gamma_s \rightarrow \alpha + \gamma_1$. For all other listed times in the table the clock is also reset when the temperature reaches 647 °C.

excursion, and mechanical perturbation on these and related properties. Such concerns have motivated a wide range of aging studies of U-Nb alloys over the last decades (References 5 through 7 and references there in).

One area of research efforts has focused on thermally activated aging of U-6Nb over the 300 to 647 °C range. As a result of the monotectoid invariant reaction on the equilibrium U-Nb phase diagram, the phase separation over this range of temperature gives rise to a rich set of time-dependent phenomena that are ultimately manifested by two lamellar phases forming out of an initially homogeneous, solute-supersaturated microstructure and, concurrently, by a large compositional swing between the initial Nb-supersaturated (γ_s) and final (γ_2) states of the bcc phases. Based on *ex situ* metallography measurements,[6] the initial aging involves general precipitation (GP) of α-U and γ_1 that forms non-lamellar microstructures, where γ_1 refers to the bcc phase having intermediate Nb composition between the start of γ_s and the metastable state of $\gamma_{1\text{-}2}$, typically in the 20 to 50 at. pct Nb range, and $\gamma_{1\text{-}2}$ is a metastable composition formed as a result of discontinuous precipitation (DP). The microstructure at this stage of aging is termed non-lamellar and the precipitation of α-U in the Nb-rich bcc-phase matrix cannot be resolved by the conventional light optical metallography method. As aging continues, the microstructures are replaced with a fine lamellar spacing (> 40 nm) when DP starts consuming the GP product. The final equilibrium state is achieved with a secondary lamellar reaction of discontinuous coarsening (DC) that sweeps through the microstructure and replaces the fine lamellar microstructure with lamellae that are 5 to 10 times coarser, and with a change in γ-phase composition called γ_2 that approaches ~ 75 at. pct Nb. All these reactions are first-order diffusional transformations that are generally described by roughly equivalent terms such as cellular reaction, DP and lamellar reaction.[8] Over the past years, the *ex situ* metallography techniques have widely been used to study the time-dependent phase and microstructure evolution over wide ranges of time and temperature, including time–temperature–transformation (TTT) diagram,[9] metastable U-Nb phase diagram,[5] cooling-rate dependent transformations and microstructures,[4,10] overall transformation kinetics and lamellar growth kinetics,[6,11] lattice parameters,[9,12] and solute (Nb) redistribution.[11,13] A number of studies have also been carried out to determine the corresponding changes in mechanical properties at different stages of aging.[14–18] Recently, *in situ* neutron diffraction measurements were carried out on U-6Nb to monitor the phase and lattice-parameter changes during low-temperature aging.[7] These combined studies have produced a large body of information important for the understanding of aging mechanisms and for establishment of the fundamental models of constitutive behavior for U-Nb alloys. Despite all these efforts, the fine-scale crystallographic evolution during aging has not been established *in situ*, especially for the stage that precedes the DP.

In this work, we carried out combined X-ray diffraction and small-angle X-ray scattering (SAXS) measurements of U-6Nb at elevated temperatures up to 775 °C to monitor the phase evolution *in situ* and in *real-time* during heating, cooling and isothermal holding. From the diffraction experiments we determine for the first time the crystallographic details of phase transformations with sub-second time resolution, including phase and lattice-parameter evolution and solute (Nb) redistribution in the bcc phases. From the simultaneous SAXS measurements, we can also determine the time-dependent growth and coalescence of α-U domains to complement the *ex situ* metallography measurements, which will be published in a separate paper.

II. EXPERIMENTAL METHODS AND PROCEDURES

The polycrystalline ^{238}U-Nb alloy with ~ 6 wt pct Nb was used in this work. The alloy was wrought processed from Rocky Flats VAR ingot at the Union Carbide Y-12 plant in Oak Ridge. Detailed information regarding the fabrication process and Nb composition can be found in Reference 4. Pucks were then cut and machined from the homogenized ingot, encapsulated in a Cu tube, and solution-treated at 800 °C in the γ_1 phase for 4 hours followed by water quench. The diffraction experiments described below were performed on a plate-shape sample in as-machined conditions, 0.25 mm thickness and 3.0 and 4.0 mm edge lengths, which was surrounded by a tantalum foil of 10 μm and then contained inside a stainless steel containment of 35 mm height, 50 mm width and 0.4 mm thickness, welded together by electron beam. An Ambrell® EASY-HEAT induction heating system of the 10 kW capacity was used to heat the sample-containment assembly.

The time-resolved synchrotron X-ray diffraction experiments were performed using the Debye–Scherrer geometry at the high-energy beamline 1-ID-E of Advanced Photon Source, Argonne National Laboratory. The incident monochromatic X-ray beam at a wavelength of 0.17299 Å was collimated to dimensions

of 200 μm × 200 μm and passed through the sample of 0.25 mm thickness. The two dimensional diffraction patterns were collected with four fixed GE amorphous silicon flat panel detectors (*i.e.*, the Hydra), each of which covers an azimuth range of 48 deg. This detector arrangement also opens up space in the middle for simultaneous SAXS measurements. The collected 2D images were integrated into one-dimensional diffraction profiles over the 0.8275 to 2.8323 Å range using the GSAS-II. In this paper, only the data from one of the four detectors were analyzed and reported.

Shown in Figure 1 are time–temperature profiles of the experiments conducted in this work, which includes three thermal cycles on the same alloy between annealing temperatures of 750 to 775 °C and aging temperatures of 530 ± 3 °C, 526 ± 3 °C and 565 ± 4 °C. Because the control thermocouples were located at the edges of the steel plate, which is approximately 15 mm away from the sample position, the sample temperatures were calculated using the refined lattice parameters for stainless steel based on previously reported coefficients of thermal expansion (CTEs).[19] For initial heating, an average heating rate of 65 °C/s was attained between 125 °C and 400 °C; between 400 °C and 775 °C the average heating rate was 2.6 °C/s. In each of the three cooling and isothermal hold cycles, the U-6Nb sample was first solution-annealed at 750 °C to 775 °C for 35 to 50 minutes, and then cooled to a desired aging temperature. The average cooling rate attained in the first two cycles is 1.2 and 0.8 °C/s in the third one. For both heating and cooling, as well as the early stages of isothermal holds, the data were collected with 0.32 seconds time resolution. As isothermal aging continued, the data were collected with 0.6 seconds and/or 6 seconds

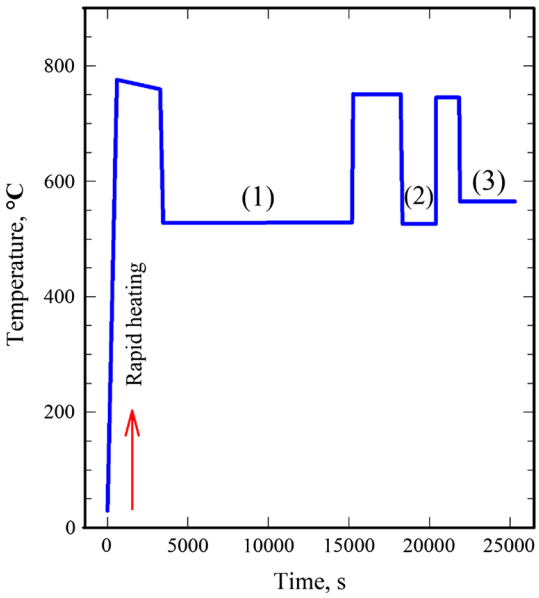

Fig. 1—Time–temperature profiles for the experiment conducted at beamline 1-ID of Advanced Photon Source. The numbers in parentheses denote three isothermal aging cycles after solution annealed at 750 °C to 775 °C. The temperatures were calculated using the refined lattices parameters for stainless steel based on the CTE reported in Ref. [19].

time resolution at different stages of aging. In all subsequent sections, the clock is reset at the onset of different stages of phase transformation and precipitation to facilitate the presentation and discussion of the time-resolved phase evolution.

The collected 1D diffraction data were analyzed using the Rietveld method with the General Structure Analysis System (GSAS) program of Larson and Von Dreele.[20] The space groups used in the refinements are *C m c m*, $C112_1/m$, *P* 4/*n m m*, and *I m* -3 *m*, respectively, for the α, α'', γ^o, and Nb-rich bcc structures. For each starting GSAS experimental file used in the automation script, the refinements typically proceeded in the following sequence when the preceding step was converged: scale factor and background coefficients (Shifted Chebyshev function); lattice parameters and phase fractions; peak profiles (pseudo-Voigt profile function built into the GSAS); atomic coordinates and atomic displacement parameters (U_{iso}), each of which were constrained to have the same values for U and Nb atoms. For Nb-supersaturated γ_s and martensitic phases of α'' and γ^o, the atom fractions were fixed at 0.86 and 0.14, respectively, for U and Nb atoms. When phase decomposition occurs during isothermal holding the atom fractions in the γ_1 and $\gamma_{1\text{-}2}$ phases were fixed at 0.5 each for U and Nb atoms, which would introduce errors in the refined weight fractions up 0.02 assuming that the precipitated bcc phases span a composition range of 20 to 80 at. pct Nb between the start (γ_1) and final equilibrium state (γ_2) of phase decomposition. At each isothermal temperature the Nb contents in the bcc phases (γ_s, γ_1 and $\gamma_{1\text{-}2}$) were determined from the refined lattice parameters based on a Vegard's-type relationship.[21] In this paper, the data analysis and related discussion are focused on the initial heating stage up to ~ 500 °C and thermal cycles 1 and 3 shown in Figure 1.

III. RESULTS AND DISCUSSION

A. *Reverse Martensitic Transformations of U-6Nb During Rapid Heating*

The monoclinic α'', tetragonal γ^o and bcc γ_s phases of U-6Nb can readily be distinguished based on their respective diffraction patterns and substantial differences in the reflection multiplicity between involved phases. Examples of diffraction patterns and refinements are shown in Figure 2(a) for the starting α'' phase at ambient temperature and in Figure 2(b) for the onset of the $\alpha'' \rightarrow \gamma^o$ transformation, which is bracketed between 161 °C and 185.2 °C based on the visual inspection of the first appearance of the characteristic (111) diffraction line for the γ^o phase. At 185.2 °C, the refined unit-cell volumes for the coexisting α'' and γ^o phases are, respectively, 84.35(4), and 84.04(6) Å^3, and the calculated relative volume change is comparable to those previously reported for the $\alpha'' \rightarrow \gamma^o$ transformation.[22,23] As shown in Figure 3, a reverse martensitic transformation sequence $\alpha'' \rightarrow \gamma^o \rightarrow \gamma_s$ was observed upon initial and rapid heating from 125 °C to 400 °C, which took place in a flash of less than 4 seconds. The

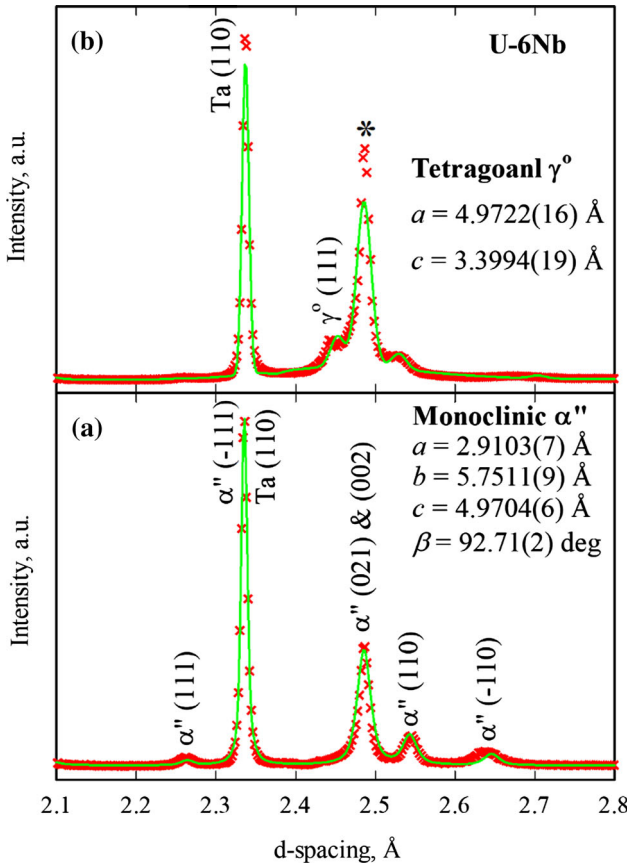

Fig. 2—Diffraction profiles showing (*a*) the starting monoclinic α″ U-6Nb and (*b*) the onset of $\alpha'' \rightarrow \gamma^{o}$ transformation at 185.2 °C. The data are shown as red crosses and the best fits based on the Rietveld refinements are shown as green curves. The asterisk denotes the overlapped peaks of α″ (002)/(021) and γ^{o} (002) (Color figure online).

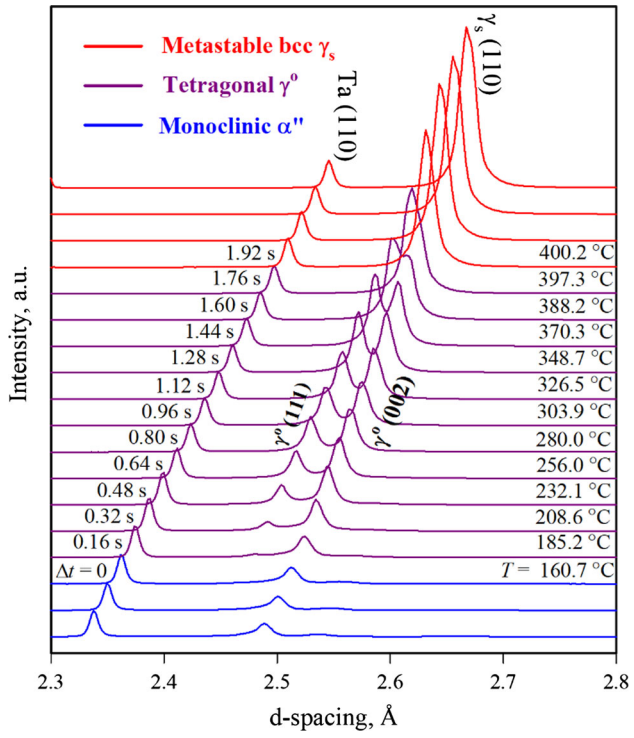

Fig. 3—Selected synchrotron X-ray diffraction data of the sub-second time resolution for U-6Nb reveal a reverse martensitic transformation, $\alpha'' \rightarrow \gamma^{o} \rightarrow \gamma_s$, upon rapid heating from 125 °C to 400 °C; the Δt in the plot is arbitrarily reset to show the time scale of the transformation sequence. The peak positions and corresponding Miller indexes for the tetragonal γ^{o} phase are based on the *P* 4/*n m m* space group and lattice parameters shown in Figs. 2(b) and 4.

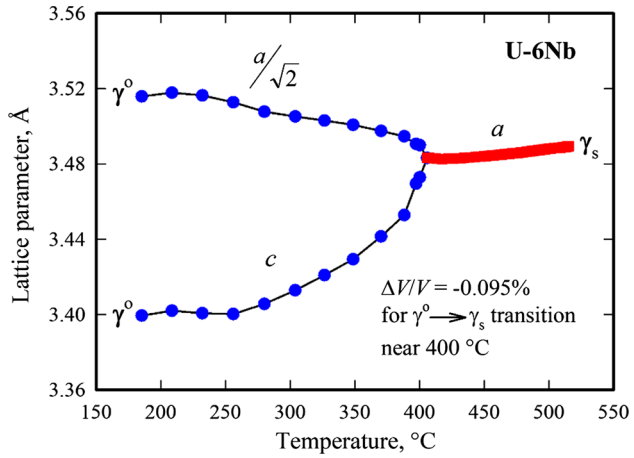

Fig. 4—Variation of lattice parameters as a function of temperature for the $\gamma^{o} \rightarrow \gamma_s$ transformation. The errors of the data points are smaller than the size of plotted symbols. The lines are plotted for guiding the eyes.

temperature for the $\gamma^{o} \rightarrow \gamma_s$ transformation is determined to be near 400 °C based on both the visual inspection of diffraction patterns and lattice parameter variations with temperature, which will be further discussed in the next paragraph. These findings are consistent with the ambient-pressure dilatometry measurements, in the sense that the Nb-supersaturated γ^{o} and γ_s phases are formed at progressively higher temperatures on rapid heating of the α″ phase. However, in our previous neutron diffraction experiments of slower heating rates and lower time resolution, a direct transformation from α″ or γ^{o} to the metastable phase assembly of α-U + γ_1 was observed upon stepwise heating at both ambient and high pressures.[22] This comparison indicates that the measurements of high time resolution is crucial for unveiling intermediate metastable phases or phase transformations leading to their final equilibrium state. To the best of our knowledge, the present findings represent the first direct observation of the $\gamma^{o} \rightarrow \gamma_s$ transformation in diffraction-based experiments. The γ_s phase is clearly metastable as it was initially formed at the temperature about 250 °C below the monotectoid temperature of 647 °C in the U-Nb system. From the consideration of the energy balance between involved phases, this can be viewed as one of the classic examples in which an intermediate or a metastable phase is often involved when the transformation to a thermodynamically stable state is kinetically hindered. In the U-Nb system, the final equilibrium state below the monotectoid temperature (*i.e.*, α-U + γ_2) involves the diffusional

phase decomposition that is kinetically sluggish at the temperatures below 400 °C.[6] On the other hand, the reverse martensitic transformations require very little thermal activation energy.

Previous studies showed that the $\gamma_s \rightarrow \gamma^o$ transformation during cooling is a thermoelastic martensitic reaction accompanied by a small volume change, ΔV.[24] For ΔV, the data hardly exists although one report based on dilatometry measurements showed that it is negligibly small.[23] To further confirm and gain more crystallographic insight into the $\gamma^o \rightarrow \gamma_s$ transformation, the lattice parameters are plotted in Figure 4 as a function of temperature. For the γ^o phase a pseudo-cubic setting was used to facilitate comparison with the cubic γ_s phase. Evidently, as the temperature approaches 400 °C the tetragonal unit cell collapses into a cubic unit cell. At 400 °C, the extrapolated volume per atom for γ^o is 21.15 Å^3 and the measured one for γ_s is 21.13 Å^3. Consistent with earlier dilatometry measurements,[23] the relative volume reduction for the $\gamma^o \rightarrow \gamma_s$ transformation near 400 °C is negligibly small, with $\Delta V/V = -0.095$ pct. Upon further heating above ~ 500 °C, the γ_s phase started decomposing into the $\alpha + \gamma_1$ metastable state, which can be visually identified by the appearance of the α phase. However, because of the weak diffraction intensity for the precipitated γ_1 phase at this stage of phase separation it is challenging to resolve the γ_1 phase from the initial γ_s phase. Consistent with the monotectoid temperature (647 °C) in the U-Nb system, the α and γ_1 phases were completely recombined into the equilibrium γ_s phase between 635 °C and 651 °C.

B. *Phase Transformations During Isothermal Aging*

In all three thermal cycles shown in Figure 1, the U-6Nb alloy transformed to the bcc γ_s phase when solution-annealed at 750 °C to 775 °C. Upon cooling and isothermal hold at each of the three experimental temperatures, our *in situ* time-resolved measurements indicate a two-stage phase separation, the first stage for the decomposition of γ_s into α-U and γ_1, thereafter referred to as GP, and the second stage for (α-U + γ_1) to decompose into the metastable state of α-U and $\gamma_{1\text{-}2}$. During the GP stage, the two bcc phases, the parent γ_s phase and precipitated γ_1, can be well resolved with the diffraction data, as shown in Figure 5 for the data collected at 530 ± 3 °C (*i.e.*, cycle 1 in Figure 1). The simultaneous growth of α-U and γ_1 over time at the expense of the γ_s phase is also clearly revealed. Thanks to the sub-second time resolution, the start and finish times for the GP reaction can be determined with an accuracy of less than 15 seconds, but it is hard to attain better resolution unambiguously by both visual inspection and Rietveld refinements of the diffraction data. Inspection of Figure 5 also shows that the peak positions for all three coexisting phases are nearly constant during the entire course of the GP reaction. For α-U, the average volumes per atom over several hundreds of data points are 21.161(5) and 21.231(5) Å^3, respectively, at the aging temperatures of 530 ± 3 °C and 565 ± 4 °C (cycle 3 in Figure 1), where the number in the parenthesis refers to the standard deviation. This is no surprise as previous work shows that at equilibrium the solubility of Nb in the α-U phase is near zero or at most no more than 1 at. pct.[2] For $\gamma_{1\text{-}2}$ phase, the Nb content can vary in a wide range up to ~ 75 at. pct when the final equilibrium state of γ_2 is achieved,[2,3] which has strong effects on the lattice parameters due to a substantial difference between pure γ-U and pure γ-Nb, ~ 0.00175 Å per at. pct Nb based on the Vegard's-type relationship of Jackson.[21] However, during the entire course of GP, the refined lattice parameters for the γ_1 phase vary in relatively small ranges and show a general trend of decreasing with increasing aging time, from 3.4557(8) to 3.4523(3) Å at 530 ± 3 °C and from 3.4604(8) to 3.4579(3) Å at 565 ± 4 °C.

To quantify the Nb contents in the γ_1 phases during the GP stage and minimize systematic errors in lattice parameter measurements, we adopted the Vegard's-type relationship of Jackson[21] using γ_s U-6Nb or 14 at. pct Nb as a reference point, which is given by

$$\text{at. pct Nb in } \gamma_1 = 14 + 100 \times [a(\gamma_s) - a(\gamma_1)]/0.175, \quad [1]$$

where at. pct Nb represents the average Nb contents in the γ_1 phase. $a(\gamma_s)$ is the lattice parameter of γ_s U-6Nb at a given aging temperature immediately prior to the GP, which is measured directly in the present experiments, 3.484 Å at 530 °C and 3.487 Å at 565 °C. The $a(\gamma_1)$ is the lattice parameter of γ_1 at a given aging time. Over

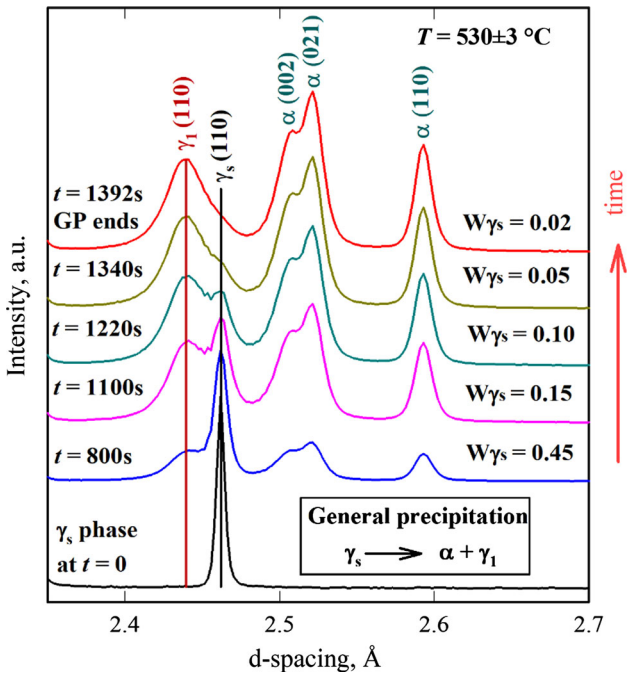

Fig. 5—Representative diffraction patterns collected during the first stage of isothermal phase decomposition at 530 °C (cycle 1 in Fig. 1), *i.e.*, $\gamma_s \rightarrow \alpha$-U + γ_1. Essentially the same phase evolution was observed at the aging temperatures of 526 °C (cycle 2) and 565 °C (cycle 3) except the different length of time between the GP start and GP end (see Table I). $W\gamma_s$ refers to the refined weight fractions for the γ_s phase, and the corresponding errors are typically within 5 pct of the listed values.

the entire course of GP at 530 ± 3 °C and 565 ± 4 °C, the Nb contents calculated from Eq. [1] for the γ_1 phase are, respectively, in a narrow range of 30.2 to 32.1 and 29.2 to 30.6 at. pct, as exemplified in Figure 6. No data are plotted for the first 120 seconds because the refinements cannot resolve the precipitated γ_1 phase from the initial γ_s phase, primarily due to the weak intensity of the γ_1 phase at the earliest stage of the transformation. Similarly, the lattice parameters and Nb contents in the γ_s phase are nearly constant during the GP stage, and the calculated mean values over several hundreds of data points are 14.76(10) at. pct at 530 ± 3 °C and 14.52(16) at. pct at 565 ± 4 °C.

Summarized in Table I is the time–temperature information for the GP reaction during the early stages of isothermal holding. The corresponding illustration in the TTT diagram is plotted in Figure 7 along with the martensitic transformations described in Section I. At all three temperatures the start of the GP reaction is defined by the first and simultaneous appearance of α-U and γ_1 based on the visual inspection of the diffraction patterns, which provides an upper bound for the incubation time. The degree of the transformation at a given time is calculated by

$$x(t) = (W\alpha + W\gamma_1)/(W\gamma_s + W\alpha + W\gamma_1), \qquad [2]$$

where $W\gamma_s$, $W\alpha$, and $W\gamma_1$ are the weight fractions of γ_s, α-U, and γ_1 phases, respectively, obtained from the Rietveld refinements. At such defined GP start the calculated values for x are in the range of 8 to 10 pct. The end of the GP is defined by the time at which the x values for γ_s start to level off around 0.02, corresponding to 98 pct transformation. Near this value, as exemplified in Figure 5, the visual inspection of the diffraction patterns also shows diminishing intensity for the γ_s phase.

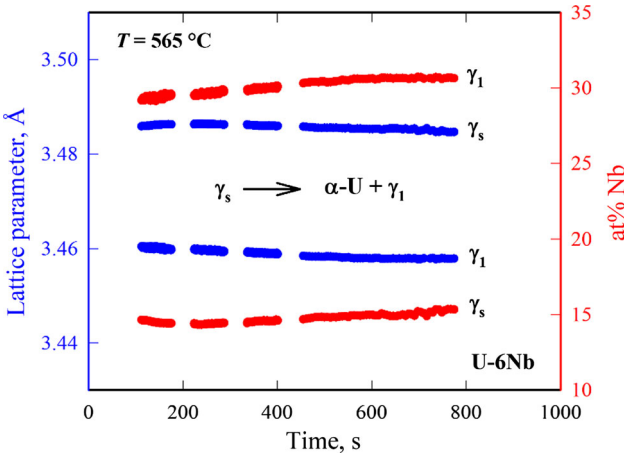

Fig. 6—Variations of lattice parameters and the corresponding Nb contents in γ_s and γ_1 phases during the first stage of isothermal phase decomposition at 565 ± 4 °C, *i.e.*, $\gamma_s \rightarrow$ α-U + γ_1. The errors of the data points are smaller than the size of plotted symbols. For the first ~ 400 s it took about 48 s to save each set of 200 frames of data that were collected with 0.32 s time resolution. The gaps in time correspond to the data saving time.

Because the cooling rates attained in this work, ranging from 0.8 to 1.2 °C/s, are substantially slower than those of water and oil quench, the GP reaction in the first two cooling cycles actually started approximately 50 seconds before the desired aging temperatures were reached. Shown in Figure 8 is one example of the cooling profiles for the isothermal aging at 530 °C. To define the incubation time for the isothermal transformation in the simplest possible way, the clock is reset to zero in each of the three cooling cycles when the temperature reached the monotectoid temperature of 647 °C, below which the γ_s phase is thermodynamically unstable. Based on this reference time, the γ_s phase remains stable in a time span of ~ 50 seconds (*i.e.*, the incubation time), and then started decomposing into α-U and γ_1 when the temperatures gradually approached the final aging temperatures of 530 ± 3 °C and 526 ± 3 °C. Both temperatures are close to the nose temperature of the TTT diagram of U-6Nb based on previous *ex situ* metallography measurements[9] and hence, thermodynamically and kinetically most favored for the diffusional phase decomposition to occur. Near these temperatures, the previously reported incubation time was less than 60 seconds, comparable to the incubation time determined in the present work. In the third cooling cycle, the incubation time was determined to be ~ 100 seconds for isothermal transformation at 565 ± 4 °C, about twice that at 530 ± 3 °C and 526 ± 3 °C yet expected from the TTT diagram of Jackson.[9] Consistent with the Arrhenius equation for the reaction rate, the determined times for the

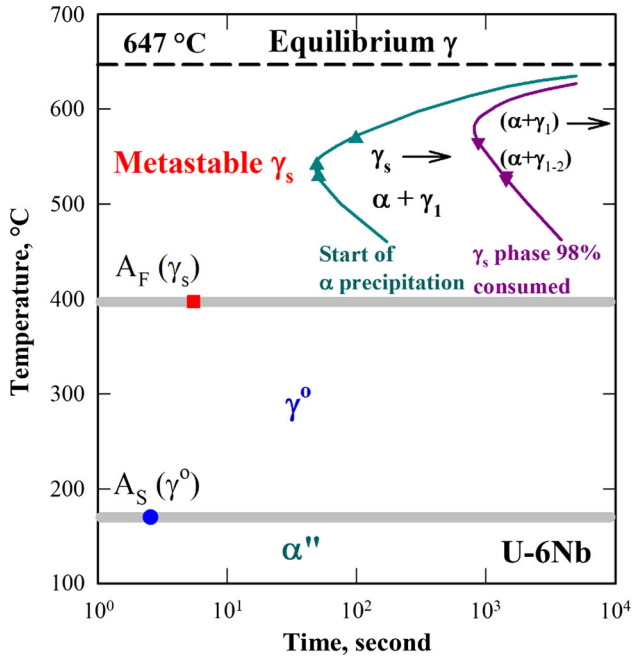

Fig. 7—TTT diagram of U-6Nb constructed based on the martensitic transformations discussed in Section I and Table I for the general precipitation reaction. The two C-curves for the start and finish of the GP are highly speculative due to the limited experimental data, and they are drawn for guiding the eyes only following the general trends of the C-curves in Ref. [9].

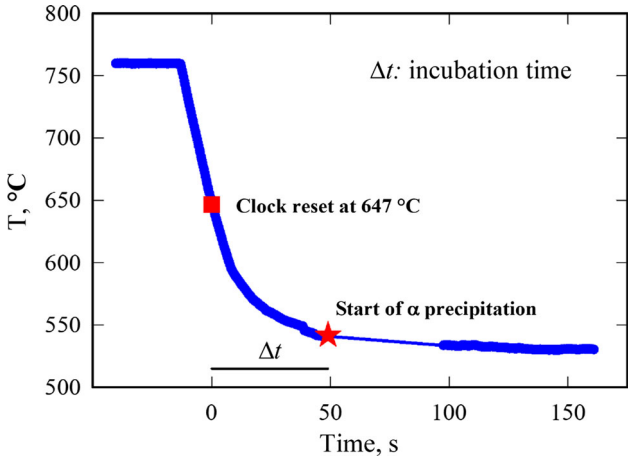

Fig. 8—A detailed thermal profile for the sample cooled from the solution-annealed temperature (760 °C) to the isothermal aging temperature of 530 °C (cycle 1 in Fig. 1).

completion of the GP reaction at 530 ± 3 °C and 526 ± 3 °C are almost twice longer than that at 565 ± 4 °C.

After the γ_s phase was completely consumed at the end of GP, the diffraction intensities were observed to decrease continuously over time in γ_1 and increase in α-U (Figure 9). For γ_1, this is in striking contrast to the observations at the GP stage, which show a continuous growth of γ_1 with increasing aging time (Figure 5). Based on previous metallographic studies,[6] the phase decomposition at this stage proceeds by the reaction $(\alpha\text{-U} + \gamma_1) \rightarrow \alpha\text{-U} + \gamma_{1\text{-}2}$ or DP. Figure 9 also shows that over time the peak positions for the bcc phase gradually shift to the smaller side of *d*-spacing, indicative of a gradual niobium enrichment. However, it is not possible to resolve unambiguously the $\gamma_{1\text{-}2}$ phase formed during the DP stage from the γ_1 phase precipitated at the GP stage. As a result, only one bcc phase was included in the refinements for the subsequent discussion, and it is labeled as $\gamma_1/\gamma_{1\text{-}2}$ in Figure 9. As a result of the Nb enrichment that spans a range of the compositions due to the mixed GP–DP microstructures, the diffraction peaks broaden gradually as aging continues.

To gain detailed insight into the phase evolution during the second-stage of decomposition, we show in Figure 10 the key parameters obtained from the Rietveld refinements. As shown in Figure 10(a), the calculated volumes per atom for α-U are essentially constant over the entire course of aging, reconfirming that the α-U formed from the precipitation is of near equilibrium composition. The bcc $\gamma_1/\gamma_{1\text{-}2}$ phase, however, is non-equilibrium as lattice parameters continue to decrease with increasing aging time. The Nb contents calculated using Eq. [1] are shown in Figure 10(b) as a function of time. At the start of the second-stage decomposition, the Nb contents of $\gamma_1/\gamma_{1\text{-}2}$ are 31.5 and 29.6 at. pct, respectively, for isothermal transformations at 530 ± 3 °C and 565 ± 4 °C. The small offset, less than 1 at. pct though, between the end of GP and the start of DP is due to the different refinement setups that changed from two bcc phases to one bcc phase. As aging

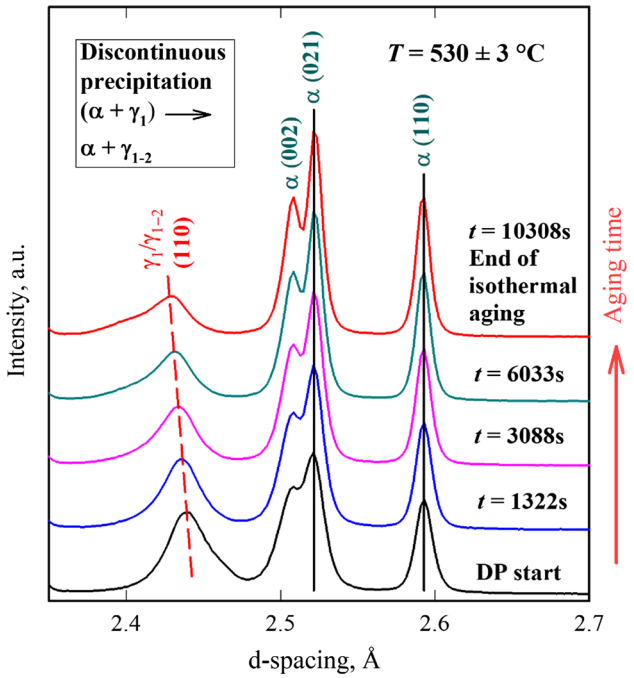

Fig. 9—Representative diffraction patterns collected during the second stage of isothermal phase decomposition (cycle 1 in Fig. 1), *i.e.*, $(\alpha + \gamma_1) \rightarrow (\alpha + \gamma_{1\text{-}2})$. Note that the γ_1 and $\gamma_{1\text{-}2}$ phases could not be resolved in the mixed GP-DP microstructures and they are labeled as $\gamma_1/\gamma_{1\text{-}2}$.

continues at 530 ± 3 °C the Nb contents increases to 47.0 at. pct over a period of 172 minutes, which, as expected, is substantially lower than the equilibrium composition of γ_2, commonly accepted to be around 75 at. pct Nb. Figure 10(c) shows the refined weight fractions of α-U and $\gamma_{1\text{-}2}$ during the second stage of isothermal decomposition. Consistent with the transformation kinetics at the GP stage, as summarized in Table I, the reaction $(\alpha\text{-U} + \gamma_1) \rightarrow \alpha\text{-U} + \gamma_{1\text{-}2}$ at 530 ± 3 °C is kinetically more sluggish than at 565 ± 4 °C. At this stage, however, it is hard to deconvolute the diffraction data that distinguish the secondary $\gamma_{1\text{-}2}$ and α-U phases from those initially precipitated at the GP stage.

C. *Kinetics of the General Precipitation*

The most general model for describing the kinetics of solid-state transformations has been developed by Avrami[25] and Erofeev[26] and is given by

$$x(t) = 1 - \exp[-(k \cdot t^n)], \qquad [3]$$

where $x(t)$ is the degree of transformation, k is the rate constant and n is a parameter that characterizes the reaction mechanism, commonly referred to as the Avrami exponent. For the diffusion controlled reaction the Avrami exponent varies between 3 and 4 for three-dimensional growth; between 3 and 2 for two-dimensional growth; and between 2 and 1 for one-dimensional growth.[27] The interpretation of the overall kinetics based on Eq. [3], however, could be problematic because in the 400 °C to 647 °C range the aging

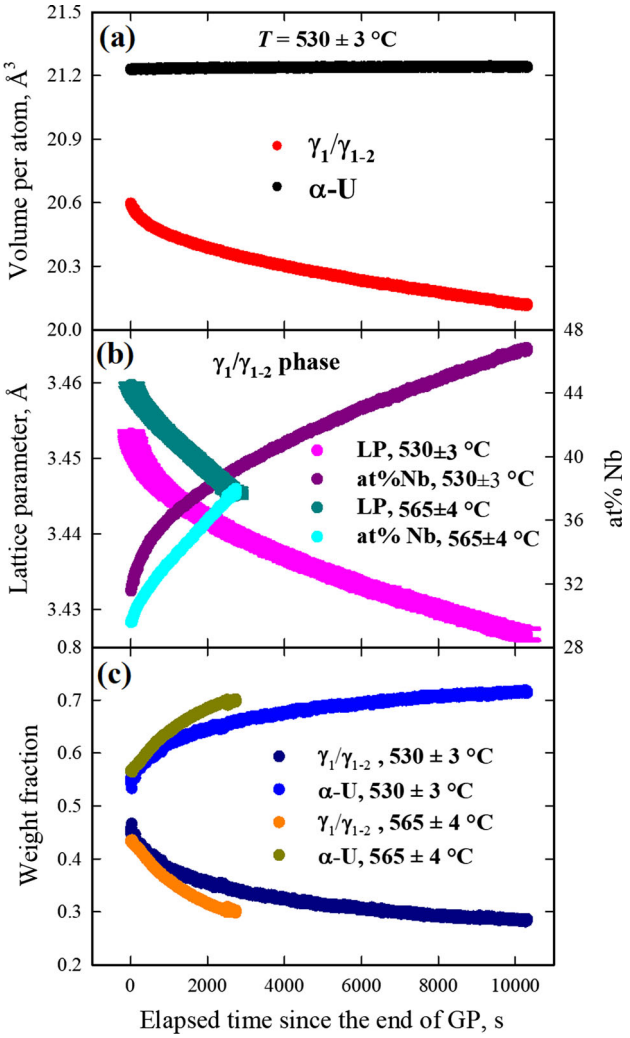

Fig. 10—The Rietveld refinement results plotted as a function of time for the second stage of isothermal transformation, *i.e.*, (α-U + γ_1) $\rightarrow$ α-U + $\gamma_{1\text{-}2}$. (*a*) Volume per atom; (*b*) lattice parameters and the corresponding Nb contents of $\gamma_{1\text{-}2}$ phase calculated according to Eq. [1]; (*c*) weight fractions. At 530 ± 3 °C (cycle 1), each plot includes 1750 data points over a period of 10,300 s. At 565 ± 4 °C (cycle 3), more than 800 data points were collected in a time span of 2735 s.

pathways in the U-Nb system are complex, and comprise three decomposition mechanisms between the initial nucleation and the final equilibrium state, non-lamellar Nb redistribution (GP), discontinuous precipitation forming fine lamellar (DP), and DC, all of which are first order diffusional phase transformations.[8] Complicating the matter further is that the GP reaction is kinetically competitive with and operates at comparable time scales as the DP reaction. In *ex situ* metallography measurements, the demarcation between transformed and untransformed regions is distinct for both the DP and DC reactions, characterized by relatively sharp interfaces separating microstructures of different length scales. For phase separation based on the diffraction data, on the other hand, the GP and DP reactions are convoluted in certain time–temperature domains, in the sense that the refined phase fractions for the α-U could include precipitations from both mechanisms. Thus, any analysis based on the Avrami rate equation is purely phenomenological and does not carry much physical meaning when two transformations overlap.

For U-Nb alloys near 6 wt pct Nb previous metallography measurements have shown that the DP reaction at 500 °C could start and interact with the GP reaction on the time scales as short as 10 to 30 minutes when isothermally aged.[6] These findings suggest that, in the present isothermal experiments at 530 °C (cycle 1) and 526 °C (cycle 2), the GP and DP and reactions could be convoluted for a portion of aging time (see time information summarized in Table I). The phase fraction data at those two temperatures are therefore not suitable for the Avrami analysis. At 550 °C, however, no lamellar microstructures characteristic of the DP reaction were observed for the first 30 minutes of aging time in *ex situ* metallography studies.[6] Based on these observations, the phase separation at 565 °C (cycle 3) is assumed to be dominated by the GP reaction for the first 13 minutes of aging, during which the initial γ_1 phase was completely consumed (see Table I). Over this period of time, the phase fraction data according to Eq. [2] are plotted in Figure 11(a). No data are plotted for the first ~ 120 seconds because the precipitated γ_1 phase cannot be resolved from the initial γ_s phase, primarily due to the weak intensity of the γ_1 phase at the early stage of the transformation. At the end of the GP, as defined in Table I, the calculated degree of the reaction according to Eq. [2] is near 0.98, which is consistent with the visual inspection of the diminishing intensity for the γ_1 phase.

Equation [3] can be rewritten as

$$\ln \ln[1/(1-x)] = \ln k + n \ln t. \qquad [4]$$

For the GP at 565 ± 4 °C, the data according to Eq. [4] are shown in Figure 11(b), which can be fitted by a straight line, suggesting that the transformation kinetics at this stage of reaction might obey the Avrami rate equation. A linear regression of the data yields $k = 3.78 \times 10^{-3}$ s^{-1} and $n = 1.024$. While extra caution needs to be exercised to interpret this phenomenological fit, the obtained Avrami exponent apparently infers a precipitation kinetics dominated by the one-dimensional growth of α-U and γ_1 nuclei, which would be plausible with a surface or grain-boundary nucleation mechanism. Further metallographic studies are needed to examine the validity of this inference.

IV. CONCLUSIONS

In summary, we have conducted *in situ* time-resolved synchrotron X-ray diffraction experiments to gain a fine-scale insight into the phase evolution of U-6Nb. Upon rapid heating from 125 °C to 400 °C, a reverse martensitic transformation sequence, $\alpha'' \rightarrow \gamma^o \rightarrow \gamma_s$, was observed for the first time in diffraction-based experiments. These observations suggest that the time-resolved measurement is crucial for unveiling intermediate

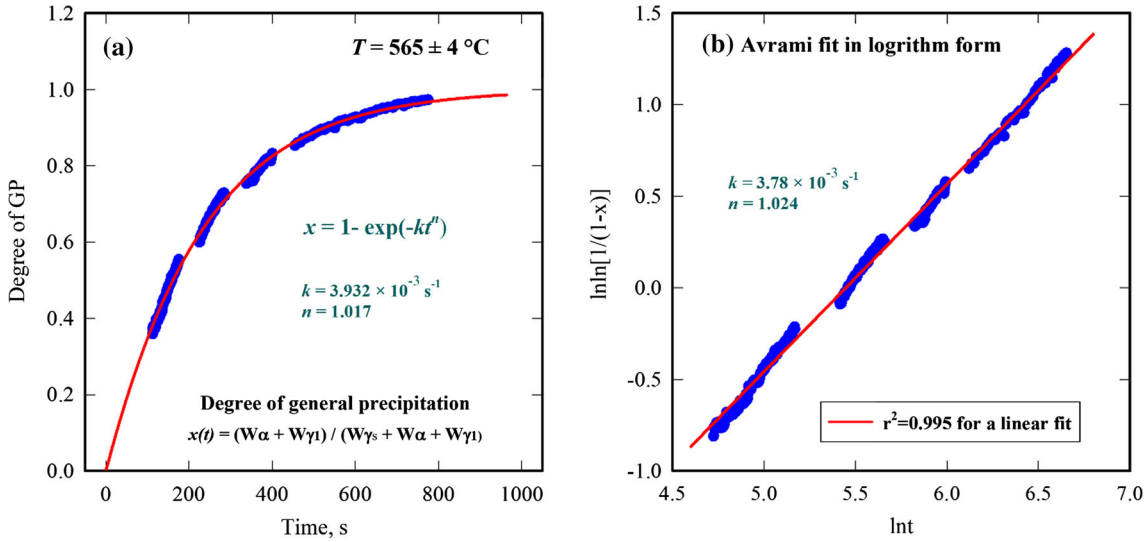

Fig. 11—(*a*) The degree of reaction plotted as a function of time for the GP reaction at 565 °C (cycle 3 in Fig 1); the red curve represents the fit using Eq. [3]. (*b*) The Avrami plot of the data of (a); the red line corresponds to the linear regression according to Eq. [4]. The gaps in time correspond to the data saving time (see Fig. 6 for more detail) (Color figure online).

metastable phases or phase transformations leading to their final equilibrium state. In three cooling/isothermal hold cycles the start and completion of the GP for the reaction $\gamma_s \rightarrow \alpha\text{-U} + \gamma_1$ can be resolved with an accuracy of a few seconds. At this stage, the Nb contents derived from a Vegard's-type relationship for γ_1 are in the 30.2 to 32.1 and 29.2 to 30.6 at. pct ranges. The precipitation kinetics during the GP stage can be described by the classic Avrami rate equation and is dominated by the one-dimensional growth of α-U and γ_1 nuclei, indicative of a surface or grain-boundary nucleation mechanism. During the DP, the γ_1 phase continues to enrich in Nb as it evolves progressively toward the $\alpha + \gamma_{1\text{-}2}$ metastable state. Overall, we demonstrate that the *in situ* time-resolved diffraction experiments can produce new and finer-scale crystallographic information to better understand phase transformations in the U-Nb system, especially during the early stages of the martensitic transformations and diffusional phase separation.

ACKNOWLEDGMENTS

This work was supported by the US Department of Energy through the Los Alamos National Laboratory. Los Alamos National Laboratory is operated by Triad National Security, LLC, for the National Nuclear Security Administration of U.S. Department of Energy (Contract No. 89233218CNA000001). The research presented in this article was supported by the Science Campaign 4 Program. The synchrotron X-ray diffraction experiments were performed at beamline 1-ID of Advanced Photon Source (APS), a U.S. Department of Energy (DOE) Office of Science User Facility operated for the DOE Office of Science by Argonne National Laboratory under Contract No. DE-AC02-06CH11357.

REFERENCES

1. J. Lehmann and R.F. Hills: *J. Nucl. Mater.*, 1960, vol. 2, pp. 261–68.
2. J. Koike, M.E. Kassner, R.E. Tate, and R.S. Rosen: *J. Phase Equilib.*, 1998, vol. 19, pp. 253–59.
3. T.C. Duong, R.E. Hackenberg, A. Landa, P. Honarmandi, A. Talapatra, H.M. Volz, A. Llobet, A.I. Smith, G. King, S. Bajaj, A. Ruban, L. Vitos, P.E.A. Turchi, and R. Arróyave: *Calphad*, 2016, vol. 55, pp. 219–30.
4. K.H. Eckelmeyer, A.D. Romig, Jr., and L.J. Weirick: *Metall. Trans. A*, 1984, vol. 15A, p. 1319.
5. R.E. Hackenberg, D.W. Brown, A.J. Clarke, L.B. Dauelsberg, R.D. Field, W.L. Hults, A.M. Kelly, M.F. Lopez, D.F. Teter, D.J. Thoma, T.J. Tucker, C.J. Vigil, and H.M. Volz: U–Nb Aging Final Report. Los Alamos National Laboratory Report LAUR-14327, 2007.
6. R.E. Hackenberg, M.G. Emigh, A.M. Kelly, P.A. Papin, R.T. Forsyth, T.J. Tucker, and K.D. Clarke: The Surprising Occurrence of Non-steady-State Growth of Divergent Lamellar Decomposition Products in Uranium–Niobium Alloys: A Preliminary Report. Los Alamos National Laboratory Report LA-UR-12-25218, 2012.
7. D.W. Brown, M.A.M. Bourke, A.J. Clarke, R.D. Field, R.E. Hackenberg, W.L. Hults, and D.J. Thoma: *J. Nucl. Mater.*, 2016, vol. 481, pp. 164–75.
8. I. Manna, S.K. Pabi, and W. Gust: *Int. Mater. Rev.*, 2001, vol. 46, pp. 53–91.
9. R.J. Jackson: Rocky Flats Plant Report RFP-1609, 1971.
10. R.A. Vandermeer: *Acta Metall.*, 1980, vol. 28, pp. 383–93.
11. R.E. Hackenberg, H.M. Volz, P.A. Papin, A.M. Kelly, R.T. Forsyth, T.J. Tucker, and K.D. Clarke: *Solid State Phenom.*, 2011, vols. 172–174, pp. 555–60.
12. H.M. Volz, R.E. Hackenberg, A.M. Kelly, W.L. Hults, A.C. Lawson, R.D. Field, D.F. Teter, and D.J. Thoma: *J. Alloys Compds*, 2007, vols. 444–445, pp. 217–25.
13. A.J. Clarke, R.D. Field, R.E. Hackenberg, D.J. Thoma, D.W. Brown, D.F. Teter, M.K. Miller, K.F. Russell, D.V. Edmonds, and G. Beverini: *J. Nucl. Mater.*, 2009, vol. 393, pp. 282–91.
14. D.W. Brown, M.A.M. Bourke, P.S. Dunn, R.D. Field, M.G. Stout, and D.J. Thoma: *Metall. Mater. Trans. A*, 2001, vol. 32A, pp. 2219–28.
15. C.M. Cady, G.T. Gray, III, S.R. Chen, R.D. Field, D.R. Korzekwa, R.S. Hixson, and M.F. Lopez: *J. Phys. IV Fr.*, 2006, vol. 134, pp. 203–08.
16. C.M. Cady, G.T. Gray, III, S.R. Chen, E.K. Cerreta, C.P. Trujillo, M.F. Lopez, R.M. Aikin, Jr., D.R. Korzekwa, and A.M. Kelly: *DYMAT*, 2009, vol. 2009, pp. 1045–51.

17. C.N. Tupper, D.W. Brown, R.D. Field, T.A. Sisneros, and B. Clausen: *Metall. Mater. Trans. A*, 2012, vol. 43A, pp. 520–30.
18. R.E. Hackenberg, R.M. Aikin, A.M. Kelly, R.T. Forsyth, P.A. Papin, D.J. Alexander, T.J. Tucker, W.L. Hults, and M.F. Lopez: Microstructure and Mechanical Response of U–6Nb and U–8Nb in Gamma Quenched and Long-Term Aged Conditions. Los Alamos National Laboratory Report LA-14487, 2016.
19. P.D. Desai and C.Y. Ho: Thermal Linear Expansion of Nine Selected AISI Stainless Steels. CINDAS-RP-51, 1978.
20. A.C. Larson and R.B. Von Dreele: GSAS—General Structure Analysis System. Los Alamos National Laboratory Report LAUR 86-748, 2000.
21. R.J. Jackson: Rocky Flats Plant Report RFP-1535, 1970.
22. J. Zhang, S.C. Vogel, D.W. Brown, B. Clausen, and R.E. Hackenberg: *J. Appl. Phys.*, 2018, vol. 123, p. 175103.
23. R.A. Vandermeer, J.C. Ogle, and W.B. Snyder: *Scripta Metall.*, 1978, vol. 12, pp. 243–48.
24. R.A. Vandermeer, J.C. Ogle, and W.G. Northcutt: *Metall. Trans. A*, 1981, vol. 12A, pp. 733–41.
25. M. Avrami: *J. Chem. Phys.*, 1939, vol. 7, pp. 1103–12.
26. B.V. Erofeev: *C. R. Acad. Sci. USSR*, 1946, vol. 52, p. 511.
27. J.W. Christian: *The Theory of Transformations in Metals and Alloys*, 1st ed., Pergamon, Oxford, 1965.